AIAA JOURNAL
Vol. 38, No. 10, October 2000

Proper Orthogonal Decomposition Technique for Transonic Unsteady Aerodynamic Flows

Kenneth C. Hall,* Jeffrey P. Thomas,† and Earl H. Dowell‡
Duke University, Durham, North Carolina 27708-0300

A new method for constructing reduced-order models (ROM) of unsteady small-disturbance flows is presented. The reduced-order models are constructed using basis vectors determined from the proper orthogonal decomposition (POD) of an ensemble of small-disturbance frequency-domain solutions. Each of the individual frequency-domain solutions is computed using an efficient time-linearized flow solver. We show that reduced-order models can be constructed using just a handful of POD basis vectors, producing low-order but highly accurate models of the unsteady flow over a wide range of frequencies. We apply the POD/ROM technique to compute the unsteady aerodynamic and aeroelastic behavior of an isolated transonic airfoil and to a two-dimensional cascade of airfoils.

Nomenclature

$\boldsymbol{A}$ = matrix defining homogeneous part of discretized aerodynamic operator
$\mathcal{A}$ = reduced-order form of $\boldsymbol{A}$
a = nondimensional location of elastic axis aft of midchord, e/b
$\boldsymbol{B}_0, \boldsymbol{B}_1$ = matrices relating airfoil motion $\boldsymbol{h}$ and $\dot{\boldsymbol{h}}$ to $\boldsymbol{b}$
b = airfoil semichord
$\boldsymbol{b}$ = vector defining inhomogeneous part of discretized aerodynamic operator
$\boldsymbol{C}$ = matrix relating small-disturbance solution $\boldsymbol{q}$ to aerodynamic force $\boldsymbol{f}$
c = airfoil chord
e = distance of elastic axis aft of airfoil midchord
$\hat{e}$ = specific internal energy
$\boldsymbol{F}, \boldsymbol{G}$ = x and y flux vectors
$\boldsymbol{f}$ = vector of aerodynamic forces acting on airfoil
G = cascade gap-to-chord ratio
h = airfoil typical section plunging degree of freedom
$\boldsymbol{h}$ = vector of airfoil displacements
$\hat{h}$ = specific enthalpy
$\boldsymbol{I}$ = identity matrix
I_α = moment of inertia of airfoil section
J = number of nodes (or cells) in computational grid
j = $\sqrt{-1}$
K = number of proper orthogonal decomposition (POD) vectors in reduced-order model
$\boldsymbol{K}$ = stiffness matrix of typical section aeroelastic model
k_h = bending stiffness of typical section aeroelastic model
k_α = torsional stiffness of typical section aeroelastic model
L = sectional airfoil lift
M = number of solution snapshots, Mach number
$\boldsymbol{M}$ = mass matrix of typical section model
M_α = aerodynamic pitching moment
m = mass per unit span of typical section aeroelastic model
N = number of degrees of freedom in computational fluid dynamics (CFD) model
$\boldsymbol{N}$ = vector operator defined by small-disturbance CFD model
$\hat{p}$ = static pressure
$\boldsymbol{Q}$ = vector containing steady flow solution
$\boldsymbol{q}$ = vector containing small-disturbance flow solution
$\boldsymbol{R}$ = nonlinear vector operator defined by steady CFD model
r = magnitude of Laplace variable s
r_α = radius of gyration divided by b
$\boldsymbol{S}$ = matrix containing solution snapshots
S_α = static imbalance of airfoil typical section
s = Laplace variable, $j\omega$
t = time
$\boldsymbol{U}$ = vector of steady conservation variables
U_∞ = freestream velocity
$\boldsymbol{u}$ = vector of unsteady small-disturbance conservation variables
$\hat{u}, \hat{v}$ = x and y components of velocity
$\hat{\boldsymbol{u}}$ = vector of unsteady nonlinear conservation variables
V = reduced velocity, $U_\infty / \omega_\alpha b \sqrt{\mu}$
$\boldsymbol{v}$ = POD eigenvector
x, y = Cartesian coordinates
x_α = static imbalance divided by b
α = airfoil typical section pitching degree of freedom
γ = ratio of specific heats
Θ = cascade stagger angle
θ = angle made by Laplace variable s in complex plane, where s is $re^{j\theta}$
λ = POD eigenvalue
μ = mass ratio, $m/\pi\rho_\infty b^2$
ξ = aerodynamic state variable
$\boldsymbol{\xi}$ = vector of aerodynamic state variables
Π = quantity extremized to find POD vectors
$\hat{\rho}$ = static density
σ = interblade phase angle of cascade vibration
$\boldsymbol{\Phi}$ = matrix of POD vectors
ϕ = POD vector
ω = frequency
$\bar{\omega}$ = reduced frequency, $\omega c/U_\infty$

Subscripts

h = plunging mode
α = pitching mode
∞ = freestream conditions

Superscript

H = Hermitian transpose

Presented as Paper 99-0655 at the 37th Aerospace Sciences Meeting, Reno, NV, 11–14 January 1999; received 22 January 1999; revision received 20 March 2000; accepted for publication 20 March 2000.

*Associate Professor, Department of Mechanical Engineering and Materials Science. Associate Fellow AIAA.
†Research Assistant Professor, Department of Mechanical Engineering and Materials Science. Member AIAA.
‡Professor, Department of Mechanical Engineering and Materials Science, and Dean Emeritus, School of Engineering. Fellow AIAA.

I. Introduction

UNSTEADY aerodynamic theories and computational fluid dynamic (CFD) models for the computation of unsteady flows about airfoils, wings, and turbomachinery cascades are quite complex, even for relatively simple flow models. Furthermore, the forms

of these analytical and computational flow models, most often cast in the time or frequency domain, are not well suited for the direct computation of aeroelastic stability, nor are they well suited for applications involving active control. Analytical models are usually formulated in the frequency domain for real frequencies, and, therefore, the aerodynamic transfer function is not composed of simple poles and zeros. For example, the Theodorsen function has a branch cut with a branch point at the origin of the Laplace plane. CFD models, on the other hand, may have many thousands of degrees of freedom, making them unwieldy for aeroelastic stability and control computations.

Investigators have developed a number of techniques to reduce the complexity of unsteady aerodynamic models. Jones[1] approximated indicial lift functions with series of exponentials in time. Such series have particularly simple Laplace transforms, that is, rational polynomials in the Laplace variable s, making them especially useful for aeroelastic computations. Padé approximants are rational polynomials whose coefficients are found by least-squares curve fitting the computed aerodynamic loads computed over a range of frequencies. Vepa,[2] Edwards,[3] and Karpel[4] developed various forms of the matrix Padé approximant technique. This approach reduces the number of so-called augmented states needed to model the various unsteady aerodynamic transfer functions (lift due to pitching, pitching moment due to pitching, etc.) by requiring that all of the transfer functions share common poles.

Hall,[5] Hall et al.,[6] Florea and Hall,[7] and Romanowski and Dowell[8] have developed reduced-order unsteady aerodynamic models of flows about airfoils, wings, and turbomachinery cascades. Using this approach, the dominant eigenvalues and eigenmodes of a time-domain or frequency-domain CFD model of unsteady flow are computed. The eigenmodes are then used as basis vectors for the construction of reduced-order models. This eigenmode reduction technique works well provided one or multiple static corrections are applied to account for the eigenmodes not retained in the reduced-order model. For a review of the eigenmode reduction technique, see Dowell et al.[9]

More recently, a number of researchers have used the proper orthogonal decomposition (POD) technique, also known as Karhunen–Loève (see Ref. 10) expansions, to determine and model coherent structures in turbulent flowfields. Lumley[11] was the first to propose using POD to uncover coherent structures in turbulent flowfields. Using this approach, one examines a series of snapshots of experimental or computational data, each at a different instant in time. These solution snapshots are used to form a small eigenvalue problem that is solved to determine a set of optimal basis functions for representing the flowfield. Other examples include work by Berkooz et al.,[12] Poje and Lumley,[13] Sirovich,[14–16] Moin and Moser,[17] Rempfer and Fasel,[18,19] and Deane et al.[20] A recently published book by Holmes et al.[21] provides an overview of the POD method along with extensive details of how the method has been used by researchers to study a wide variety of fluids problems.

A number of researchers have used the time-domain POD technique to construct reduced-order models (ROM) of unsteady aerodynamic flows. Romanowski,[22] for example, has used the POD technique to create a reduced-order aeroelastic model of a two-dimensional isolated airfoil, including compressible aerodynamics. Romanowski has shown that very accurate unsteady flow models can be constructed that reduce the number of degrees of freedom from the thousands associated with the original CFD flow solver to a few tens of degrees of freedom. Tang et al.[23] have used the POD technique to create an ROM of vortex shedding from a cylinder. They proposed that the ROM could then be used to design an active control system to control the shedding.

Most of the previous work using POD used data sampled from the time domain or from ensembles of steady data, as in the case of graphical feature recognition. Recently, however, Kim[24] developed a frequency-domain form. Using this approach, snapshots of the unsteady flow are computed at a number of discrete frequencies rather than at discrete instants in time. He applied the technique to two relatively simple dynamic systems: a 12-degree-of-freedom mass–spring damper system and an incompressible three-dimensional vortex lattice model of a rectangular wing.

In this paper, we develop a frequency-domain form of the POD technique. Here, we use time-linearized CFD analyses to compute unsteady small-disturbance flow solutions for vibrating airfoils in the frequency domain over a range of frequencies. Basis vectors are then extracted from this frequency-domain data set using the POD technique. The resulting basis vectors are then used to construct low-degree-of-freedom ROMs of the unsteady flow. Finally, the reduced-order aerodynamic model is combined with a structural dynamic model resulting in a compact, but accurate, flutter model. In this paper, we apply the technique to a two-dimensional transonic airfoil and also to a two dimensional cascade of vibrating airfoils. Although the results presented here are two dimensional, the method itself is general and can be readily extended to three-dimensional flows.

II. Theory

A. Steady and Small-Disturbance Unsteady Flow Models

Although the POD technique may be applied to a wide range of linear and nonlinear flow problems, in this paper we consider only small-disturbance unsteady two-dimensional inviscid flows. Thus, we consider the time-dependent two-dimensional Euler equations, which may be expressed as

$$\frac{\partial \hat{\boldsymbol{u}}}{\partial t} + \frac{\partial \boldsymbol{F}(\hat{\boldsymbol{u}})}{\partial x} + \frac{\partial \boldsymbol{G}(\hat{\boldsymbol{u}})}{\partial y} = \boldsymbol{0} \tag{1}$$

where $\hat{\boldsymbol{u}}$ is the vector of conservation variables given by

$$\hat{\boldsymbol{u}}(x, y, t) = \begin{Bmatrix} \hat{\rho} \\ \hat{\rho}\hat{u} \\ \hat{\rho}\hat{v} \\ \hat{\rho}\hat{e} \end{Bmatrix} \tag{2}$$

and $\hat{e}$ is the total specific energy. The flux vectors $\boldsymbol{F}$ and $\boldsymbol{G}$ are given by

$$\boldsymbol{F}(\hat{\boldsymbol{u}}) = \begin{Bmatrix} \hat{\rho}\hat{u} \\ \hat{\rho}\hat{u}^2 + \hat{p} \\ \hat{\rho}\hat{u}\hat{v} \\ \hat{\rho}\hat{u}\hat{h} \end{Bmatrix}, \qquad \boldsymbol{G}(\hat{\boldsymbol{u}}) = \begin{Bmatrix} \hat{\rho}\hat{v} \\ \hat{\rho}\hat{u}\hat{v} \\ \hat{\rho}\hat{v}^2 + \hat{p} \\ \hat{\rho}\hat{v}\hat{h} \end{Bmatrix} \tag{3}$$

where the specific enthalpy $\hat{h}$ is

$$\hat{h} = (\hat{\rho}\hat{e} + \hat{p})/\hat{\rho} \tag{4}$$

and, for a calorically perfect gas, the pressure $\hat{p}$ is given by

$$\hat{p} = (\gamma - 1)[\hat{\rho}\hat{e} - (\hat{\rho}/2)(\hat{u}^2 + \hat{v}^2)] \tag{5}$$

In the present investigation, we are interested in small-disturbance, harmonically varying unsteady flows about some nonlinear mean operating condition. Thus, we assume the conservative variables $\hat{\boldsymbol{u}}$ may be expanded in a perturbation series of the form

$$\hat{\boldsymbol{u}}(x, y, t) = \boldsymbol{U}(x, y) + \boldsymbol{u}(x, y)\, e^{j\omega t} \tag{6}$$

where $\boldsymbol{U}(x, y)$ represents for a given problem the steady background flow, which is also a solution to Eq. (1). Also, $\boldsymbol{u}(x, y)$ is the complex amplitude of the small-disturbance unsteady flow that arises from an external excitation with frequency ω.

Substituting Eq. (6) into the nonlinear Euler equations, Eq. (1) and expanding the result in a perturbation series in the small-disturbance quantities, one finds that, to zeroth order, the governing equations are given by

$$\frac{\partial \boldsymbol{F}(\boldsymbol{U})}{\partial x} + \frac{\partial \boldsymbol{G}(\boldsymbol{U})}{\partial y} = \boldsymbol{0} \tag{7}$$

This vector equation (the steady Euler equations) describes the steady background flow. The first-order equation describes the small-disturbance unsteady flow and is given by

$$j\omega\boldsymbol{u} + \frac{\partial}{\partial x}\left(\frac{\partial \boldsymbol{F}}{\partial \boldsymbol{U}}\boldsymbol{u}\right) + \frac{\partial}{\partial y}\left(\frac{\partial \boldsymbol{G}}{\partial \boldsymbol{U}}\boldsymbol{u}\right) = \boldsymbol{0} \tag{8}$$

where, for example,

$$\frac{\partial \boldsymbol{F}}{\partial \boldsymbol{U}} = \left.\frac{\partial \boldsymbol{F}(\hat{\boldsymbol{u}})}{\partial \hat{\boldsymbol{u}}}\right|_{\hat{\boldsymbol{u}}=\boldsymbol{U}} \tag{9}$$

Equations (7) and (8) are solved sequentially, with boundary conditions that depend on the particular physical problem to be solved. For problems involving airfoil vibration, for example, as in the case of a flutter calculation, a deforming computational grid that conforms to the motion of the airfoil may be used to improve the accuracy of the unsteady flow solution. In this case, Eq. (8) will contain an additional inhomogeneous term that is dependent on the grid deformation and the mean flow.[25]

B. Numerical Discretization Scheme

The starting point for the construction of a POD-based ROM is a conventional CFD scheme. In this study, we use time-linearized, that is, frequency-domain, small-disturbance flow solvers. In the present investigation, we use two different discretization schemes; one is a cell-centered, explicit, finite volume Godunov[26] method using Roe's[27] approximate Riemann solver with van Leer's[28] technique for preserving monotonicity. The other is a node-centered Lax–Wendroff scheme (see Ref. 29). The steady Euler and unsteady time-linearized Euler equations are discretized on a computational mesh composed of quadrilateral cells. At the center of the jth cell of the computational grid for a cell-centered scheme, or the jth node of a node-centered scheme, the estimate of the solution $\boldsymbol{u}$ is stored and is denoted by $\boldsymbol{u}_j$. The steady and unsteady solution for the entire computational domain may be thought of as vectors of the form

$$\boldsymbol{q} = \begin{Bmatrix} \boldsymbol{u}_1 \\ \boldsymbol{u}_2 \\ \vdots \\ \boldsymbol{u}_J \end{Bmatrix}, \qquad \boldsymbol{Q} = \begin{Bmatrix} \boldsymbol{U}_1 \\ \boldsymbol{U}_2 \\ \vdots \\ \boldsymbol{U}_J \end{Bmatrix} \tag{10}$$

where J is the total number of computational cells for a cell-centered scheme or the number of nodes for a node-centered scheme. Thus, the total number of entries N in each of the two vectors in Eq. (10) is $N = 4 \times J$.

Next, the steady and time-linearized Euler equations are discretized. The resulting discretization of the steady Euler equations for an explicit scheme can be expressed as

$$\boldsymbol{Q}^{n+1} - \boldsymbol{Q}^{n} = \boldsymbol{R}(\boldsymbol{Q}^{n}) \tag{11}$$

where n is the iteration number. To solve for the steady flow, the solution is advanced in time until a steady-state solution is obtained.

Similarly, once the steady flow has been computed, the time-linearized unsteady Euler equations are discretized with the result

$$\boldsymbol{q}^{n+1} - \boldsymbol{q}^{n} = \boldsymbol{N}(\boldsymbol{q}^{n}; \boldsymbol{Q}, \omega, \Delta) \tag{12}$$

where Δ is a shorthand notation for the particular type of external source of excitation. Note the boundary conditions themselves may be functions of ω. In other words, the unsteady flow depends on the steady flow, the frequency of the disturbance, and the type of excitation.

Although $\boldsymbol{N}$ is an operator for solving a time-linearized system of equations, $\boldsymbol{N}$ is not, strictly speaking, a linear operator because of the presence of inhomogeneous boundary conditions, that is, $\boldsymbol{N}(\boldsymbol{0}) \neq \boldsymbol{0}$. Nevertheless, the operator $\boldsymbol{N}$ may be expressed as a linear system of equations of the form

$$\boldsymbol{N}(\boldsymbol{q}; \omega, \Delta) = [\boldsymbol{A}(\omega)]\boldsymbol{q} - \boldsymbol{b}(\omega, \Delta) = \boldsymbol{0} \tag{13}$$

where $\boldsymbol{A}$ is a large sparse matrix and $\boldsymbol{b}$ is a vector arising from the imposition of unsteady inhomogeneous boundary conditions.

For the cell-centered Roe[27] scheme, the matrix $\boldsymbol{A}$ and the vector $\boldsymbol{b}$ are first order in ω. Thus, Eq. (13) can be written as

$$[\boldsymbol{A}_0]\{\boldsymbol{q}\} + j\omega[\boldsymbol{A}_1]\{\boldsymbol{q}\} = \boldsymbol{b}_0 + j\omega\boldsymbol{b}_1 \tag{14}$$

where $\boldsymbol{A}_0$ and $\boldsymbol{A}_1$ are independent of the excitation frequency ω. For the node-centered Lax–Wendroff scheme, the matrix $\boldsymbol{A}$ and the vector $\boldsymbol{b}$ are second order in ω. Thus, Eq. (13) has the form

$$[\boldsymbol{A}_0]\{\boldsymbol{q}\} + j\omega[\boldsymbol{A}_1]\{\boldsymbol{q}\} - \omega^2[\boldsymbol{A}_2]\{\boldsymbol{q}\} = \boldsymbol{b}_0 + j\omega\boldsymbol{b}_1 - \omega^2\boldsymbol{b}_2 \tag{15}$$

For unsteady flows about isolated airfoils, the matrices $\boldsymbol{A}_0$, $\boldsymbol{A}_1$, and $\boldsymbol{A}_2$ are purely real. For unsteady flows about a cascade of airfoils, the matrices may be complex due to the complex periodic boundary conditions used to impose the fixed interblade phase angle σ of a traveling wave disturbance.

In some instances, one would like to compute the homogeneous solutions of the discretized unsteady aerodynamic model. Such would be the case, for example, if one wanted to compute the onset of vortex shedding for an airfoil or rotating stall for a turbomachinery compressor. Setting the right-hand side of Eq. (14) to zero, for example, one obtains the eigenvalue problem

$$[\boldsymbol{A}_0]\{\boldsymbol{q}\} + s[\boldsymbol{A}_1]\{\boldsymbol{q}\} = \boldsymbol{0} \tag{16}$$

where the eigenvalue $s = j\omega$ will, in general, be complex, as will be the eigenvectors. For the isolated airfoil case, the complex eigenvalues (and corresponding eigenvectors) will appear in complex conjugate pairs. One should be careful when interpreting the eigenvalues of the CFD model. Some of the eigenvalues will be (nearly) equal to the eigenvalues of the physical system. Others, however, form a discrete approximation of a branch cut in the complex Laplace plane.[5]

C. Definition of POD Basis Vectors

The idea behind the frequency-domain POD technique is a simple one. We first calculate the small-disturbance response of the aerodynamic system at M different combinations of frequency and excitation. The solutions (also called snapshots) are denoted by $\boldsymbol{q}^m$ for $m = 1, 2, \ldots, M$. These snapshots are then linearly combined to form a smaller number of basis vectors ϕ_k for $k = 1, 2, \ldots, K$, where $K < M$. That is,

$$\phi_k = \sum_{m=1}^{M} \boldsymbol{q}^m v_k^m, \qquad k = 1, 2, 3, \ldots, K \tag{17}$$

where v_k^m is the contribution of the mth snapshot to the kth basis vector. In matrix form, Eq. (17) is written as

$$\phi_k = \boldsymbol{S}\boldsymbol{v}_k \tag{18}$$

where

$$\boldsymbol{S} = \begin{bmatrix} | & | & & | \\ \boldsymbol{q}^1 & \boldsymbol{q}^2 & \cdots & \boldsymbol{q}^M \\ | & | & & | \end{bmatrix} \tag{19}$$

$$\boldsymbol{v}_k = \begin{Bmatrix} v_k^1 \\ v_k^2 \\ \vdots \\ v_k^M \end{Bmatrix} \tag{20}$$

We assume here the vector $\boldsymbol{v}_k$ has been suitably scaled so that the vectors ϕ_k are unit length. The vectors $\boldsymbol{v}_k$ are selected so that they lie along the principal axes of the space spanned by $\boldsymbol{S}$; that is, the quantity

$$\left\| \boldsymbol{S}^H \boldsymbol{S}\boldsymbol{v}_k \right\|_2 \tag{21}$$

is extremized subject to the constraint that ϕ_k is unit length. Thus, introducing the Lagrange multiplier λ_k, we find the vector $\boldsymbol{v}_k$ that makes Π stationary, where

$$\Pi = \boldsymbol{v}_k \boldsymbol{S}^H \boldsymbol{S}\boldsymbol{S}^H \boldsymbol{S}\boldsymbol{v}_k - \lambda_k \left(\boldsymbol{v}_k \boldsymbol{S}^H \boldsymbol{S}\boldsymbol{v}_k - 1 \right) \tag{22}$$

Taking the variation of Π and setting the result to zero give

$$\boldsymbol{S}^H \boldsymbol{S}\boldsymbol{v}_k = \lambda_k \boldsymbol{v}_k \tag{23}$$

Equation (23) defines an eigenvalue problem for the eigenvectors $\boldsymbol{v}_k$ and eigenvalues λ_k. Those eigenvectors with the largest values of λ_k give the largest values of the quantity in Eq. (21). Said another way, the snapshots $\boldsymbol{q}^m$ tend to lie in a subspace spanned by the basis vectors ϕ_k with the largest eigenvalues λ_k.

D. Reduced-Order Aerodynamic Model

In this section, we describe a technique for constructing reduced-order aerodynamic models of CFD schemes using POD vectors. In the next section, we describe how to construct reduced-order aeroelastic models. For the sake of brevity, this development is shown only for the cell-centered Godunov scheme.[26] However, very similar analyses can applied to the node-centered Lax–Wendroff scheme with just minor modifications required because the Lax–Wendroff formulation is second order in ω.

To begin, having computed the POD basis vectors, we assume that they will provide a useful basis for computing the unsteady solution at some other frequency and/or external excitation than was used to generate the original snapshots. Thus, we let

$$\boldsymbol{q} = \sum_{k=1}^{K} \phi_k \xi_k \tag{24}$$

where ξ_k may be thought of as as an aerodynamic state variable (sometimes referred to as an augmented aerodynamic state in the Padé literature). In matrix form, Eq. (24) is given by

$$\boldsymbol{q} = \boldsymbol{\Phi}\boldsymbol{\xi} \tag{25}$$

where $\boldsymbol{\Phi}$ is an $N \times K$ matrix, whose kth column is simply the basis vector ϕ_k, and $\boldsymbol{\xi}$ is the vector of aerodynamic state variables. Substitution of Eq. (25) into Eq. (13) gives

$$\boldsymbol{A}\boldsymbol{\Phi}\boldsymbol{\xi} = \boldsymbol{b} \tag{26}$$

In practice, the matrix $\boldsymbol{A}$ is never actually computed. Instead, we compute the kth column of $\boldsymbol{A}\boldsymbol{\Phi}$ using the original linearized flow solver itself. That is,

$$\boldsymbol{A}\phi_k = \boldsymbol{N}(\phi_k) - \boldsymbol{N}(\boldsymbol{0}) \tag{27}$$

Next, we project the error in Eq. (26) onto the space spanned by the basis vectors to obtain

$$\boldsymbol{\Phi}^H \boldsymbol{A} \Phi \boldsymbol{\xi} = \mathcal{A}\boldsymbol{\xi} = \boldsymbol{\Phi}^H \boldsymbol{b} \tag{28}$$

Finally, the matrix $\mathcal{A}$ is factored using lower–upper decomposition, and Eq. (28) is solved for the unknown aerodynamic state variables $\boldsymbol{\xi}$. This step is computationally very efficient because the reduced-order matrix $\mathcal{A}$ is quite small, sometimes as small as 10×10, but rarely larger than 100×100. The major expense in constructing the aerodynamic ROM is the computation of the snapshots; the computational cost of finding the basis vectors and solution to Eq. (28) is negligible by comparison.

We note that by construction the reduced-order aerodynamic model [Eq. (28)] satisfies the boundary conditions (and the discretized field equations) only approximately. This should not be viewed as a weakness of the method, but a strength. Imposing a constraint that boundary conditions be satisfied exactly at all of the points on the boundary would require many more basis functions to be included in the model, at least as many basis vectors as boundary points, and would not substantially improve the model.

For some applications, for example, to examine the stability of the CFD model itself, it is desirable to compute the eigenvalues of the CFD model. Also, the eigenspectrum of a CFD model is a useful assessment tool in examining grid and/or modal convergence of the original CFD model and/or an associated reduced-order model.

The computational cost of computing even a few of the eigenvalues of the full CFD model of the unsteady flow [Eq. (16)] can be quite large, especially for viscous and/or three-dimensional flow models. An alternative is to compute the eigenvalues with a Ritz approach, using the POD modes as basis vectors. Recall that for the Godunov[26] flow solver the matrix $\boldsymbol{A}$ is first order in ω; the homogeneous part of Eq. (28) may be written as

$$\mathcal{A}_0\boldsymbol{\xi} + s\mathcal{A}_1\boldsymbol{\xi} = \boldsymbol{0} \tag{29}$$

where

$$\mathcal{A}_0 = \boldsymbol{\Phi}^H \boldsymbol{A}_0 \boldsymbol{\Phi}, \qquad \mathcal{A}_1 = \boldsymbol{\Phi}^H \boldsymbol{A}_1 \boldsymbol{\Phi} \tag{30}$$

Equation (29) may be used to determine the dominant eigenvalues and eigenvectors of the full CFD model, but Eq. (29) has many fewer degrees of freedom than the original system, greatly reducing the computational cost.

E. Reduced-Order Aeroelastic Model

Having described the basic reduced-order modeling technique, we next describe how to incorporate an aerodynamic ROM into an aeroelastic model of flutter. To illustrate, we again consider the Godunov[26] CFD algorithm described earlier. A similar but slightly more complicated form (not presented here) can be derived for the Lax–Wendroff scheme.

Consider a two-degree-of-freedom structural dynamic model of a typical section. The governing equations of motion are of the form

$$\boldsymbol{M}\ddot{\boldsymbol{h}} + \boldsymbol{K}\boldsymbol{h} = \boldsymbol{f} \tag{31}$$

where

$$\boldsymbol{h} = \begin{Bmatrix} h \\ \alpha \end{Bmatrix} \tag{32}$$

and h and α are the plunging and pitching degrees of freedom of the typical section. Also,

$$\boldsymbol{M} = \begin{bmatrix} m & S_\alpha \\ S_\alpha & I_\alpha \end{bmatrix}, \qquad \boldsymbol{K} = \begin{bmatrix} k_h & 0 \\ 0 & k_\alpha \end{bmatrix}, \qquad \boldsymbol{f} = \begin{Bmatrix} -L \\ M_\alpha \end{Bmatrix} \tag{33}$$

where m, S_α, and I_α are the mass, static imbalance, and moment of inertia of the airfoil section measured about the elastic axis, k_h and k_α are the bending and torsional spring constants, and L and M_α are the aerodynamic lift and moment produced by the motion of the airfoil.

Note that the aerodynamic force vector $\boldsymbol{f}$ is obtained from integrals involving the pressure at the surface of the airfoil. When discretized, these integrals may be expressed as

$$\boldsymbol{f} = \boldsymbol{C}\boldsymbol{q} \tag{34}$$

where $\boldsymbol{C}$ is a sparse $2 \times N$ matrix. Similarly, for the case of airfoil vibration, the vector $\boldsymbol{b}$ on the right-hand side of Eq. (14) can be expressed as

$$\boldsymbol{b} = \boldsymbol{b}_0 + j\omega\boldsymbol{b}_1 = \boldsymbol{B}_0\boldsymbol{h} + j\omega\boldsymbol{B}_1\boldsymbol{h} \tag{35}$$

where now we have made the assumption that the airfoil motion is harmonic in time, that is, $\boldsymbol{h} = \bar{\boldsymbol{h}}\exp(j\omega t)$ (ω may be complex). Putting together Eq. (14) and Eqs. (31–35) and converting to first order in ω (state-space form) give

$$\begin{bmatrix} \boldsymbol{A}_0 & -\boldsymbol{B}_0 & -\boldsymbol{B}_1 \\ \boldsymbol{0} & \boldsymbol{0} & \boldsymbol{I} \\ -\boldsymbol{C} & \boldsymbol{K} & \boldsymbol{0} \end{bmatrix} \begin{Bmatrix} \boldsymbol{q} \\ \boldsymbol{h} \\ \dot{\boldsymbol{h}} \end{Bmatrix} + j\omega \begin{bmatrix} \boldsymbol{A}_1 & \boldsymbol{0} & \boldsymbol{0} \\ \boldsymbol{0} & -\boldsymbol{I} & \boldsymbol{0} \\ \boldsymbol{0} & \boldsymbol{0} & \boldsymbol{M} \end{bmatrix} \begin{Bmatrix} \boldsymbol{q} \\ \boldsymbol{h} \\ \dot{\boldsymbol{h}} \end{Bmatrix} = \boldsymbol{0} \tag{36}$$

Equation (36) is a large sparse $(N + 4) \times (N + 4)$ generalized eigenvalue problem that describes the aeroelastic stability of the airfoil.

For large CFD models, finding the eigenvalues of Eq. (36) is prohibitively expensive. To reduce the size of the model, we again assume that the number of aerodynamic states can be reduced using Eq. (24), so that

$$\begin{bmatrix} \boldsymbol{A}_0\boldsymbol{\Phi} & -\boldsymbol{B}_0 & -\boldsymbol{B}_1 \\ \boldsymbol{0} & \boldsymbol{0} & \boldsymbol{I} \\ -\boldsymbol{C}\boldsymbol{\Phi} & \boldsymbol{K} & \boldsymbol{0} \end{bmatrix} \begin{Bmatrix} \boldsymbol{\xi} \\ \boldsymbol{h} \\ \dot{\boldsymbol{h}} \end{Bmatrix} + j\omega \begin{bmatrix} \boldsymbol{A}_1\boldsymbol{\Phi} & \boldsymbol{0} & \boldsymbol{0} \\ \boldsymbol{0} & -\boldsymbol{I} & \boldsymbol{0} \\ \boldsymbol{0} & \boldsymbol{0} & \boldsymbol{M} \end{bmatrix} \begin{Bmatrix} \boldsymbol{\xi} \\ \boldsymbol{h} \\ \dot{\boldsymbol{h}} \end{Bmatrix} = \boldsymbol{0} \tag{37}$$

Finally, projecting the error in the aerodynamic equations onto the space spanned by the POD basis vectors gives

$$\begin{bmatrix} \mathcal{A}_0 & -\Phi^H B_0 & -\Phi^H B_1 \\ 0 & 0 & I \\ -C\Phi & K & 0 \end{bmatrix} \begin{Bmatrix} \xi \\ h \\ \dot{h} \end{Bmatrix} + j\omega \begin{bmatrix} \mathcal{A}_1 & 0 & 0 \\ 0 & -I & 0 \\ 0 & 0 & M \end{bmatrix} \begin{Bmatrix} \xi \\ h \\ \dot{h} \end{Bmatrix} = 0 \tag{38}$$

Equation (38) is the reduced-order aeroelastic model, which is a generalized eigenvalue problem of size $(K+4)\times(K+4)$, where $K \ll N$.

Equation (38) is similar in form to that obtained using a matrix Padé approximant for the unsteady aerodynamics (e.g., Ref. 4) and has some of the same advantages of the Padé approach. Both methods produce low-degree-of-freedom models. Furthermore, both require the aerodynamic lift and moment transfer functions to share common eigenvalues (although the zeros are obviously different). This is appealing because physically the poles should be independent of the type of transfer function. However, the present approach has several advantages over the matrix Padé approximant method. The present method attempts to compute the actual aerodynamic poles, or at least the poles of a rational CFD model. The Padé approach, on the other hand, selects pole locations by the curve fitting of tabulated aerodynamic data. In fact, some Padé techniques can produce unstable aerodynamic poles, even for stable aerodynamic systems.

III. Computational Results

A. Unsteady Aerodynamic Behavior of a Transonic Isolated Airfoil

In this section, we present some typical two-dimensional steady and unsteady small-disturbance flow solutions for a simple model problem. The results presented are based on a standard aeroelastic test case proposed by AGARD to test the ability of computational methods to predict flutter of aircraft wings.[30] The airfoil used closely approximates a NACA 64A010 airfoil but is 10.6% thick to match closely the actual thickness distribution of an airfoil studied experimentally at the NASA Ames Research Center. We used several different computational grids. For calculations using the node-centered Lax–Wendroff scheme, we used computational grids with 65×33 nodes, 97×49 nodes, and 129×65 nodes. For a few sample calculations requiring the use of the cell-centered Godunov[26] scheme, we used a very coarse mesh with just 32×16 computational cells. The coarsest and finest grids are shown in Fig. 1.

Shown in Fig. 2 are the computed steady pressure distributions for several inflow Mach numbers at zero angle of attack. These solutions were computed with the node-centered Lax–Wendroff scheme using the 129×65 node computational grid. As the Mach number is increased, one observes that shocks form on the pressure and suction surfaces of the airfoil; these shocks move aft as the Mach number increases. Because the airfoil section is symmetric and at zero angle of attack, the pressure distributions on the upper and lower surfaces of the airfoil are identical.

We next consider the case of unsteady flow about a single steady flow operating condition. To test the method, we computed the unsteady small-disturbance solution using the cell-centered Godunov[26] scheme on the coarsest computational grid for a Mach number M of 0.85 at 11 reduced frequencies $\bar{\omega}$ equally spaced between 0.0 and 1.0, where here the frequency ω has been nondimensionalized by U_∞/c, where c is the aerodynamic chord and U_∞ is the freestream flow speed. In this example, we first computed the POD modes using the method described in Sec. II.C. Then, using these POD modes, we computed the unsteady aerodynamic eigenvalues and compared these approximate eigenvalues to the exact eigenvalues of the complete CFD scheme. Because of the large computational cost of computing the eigenvalues of the complete CFD model [Eq. (15)], we used a coarse grid for the present examples.

At each frequency, two solutions were computed, one for plunging motion of the airfoil and one for pitching motion about a point one-half chord upstream of the leading edge. The upwash on the airfoil associated with plunging motion solution at $\bar{\omega}=0$ is zero, and thus this solution is discarded, resulting in a total of 41 nontrivial solutions or snapshots. For negative frequencies, the small-disturbance solutions are simply complex conjugates of the solutions at the corresponding positive frequency. Thus, for no additional computational effort, we may include an additional 20 snapshots into the ensemble, that is, for $\bar{\omega}=-0.1,\ -0.2,\ldots,\ -1.0$, for a total of 41 snapshots.

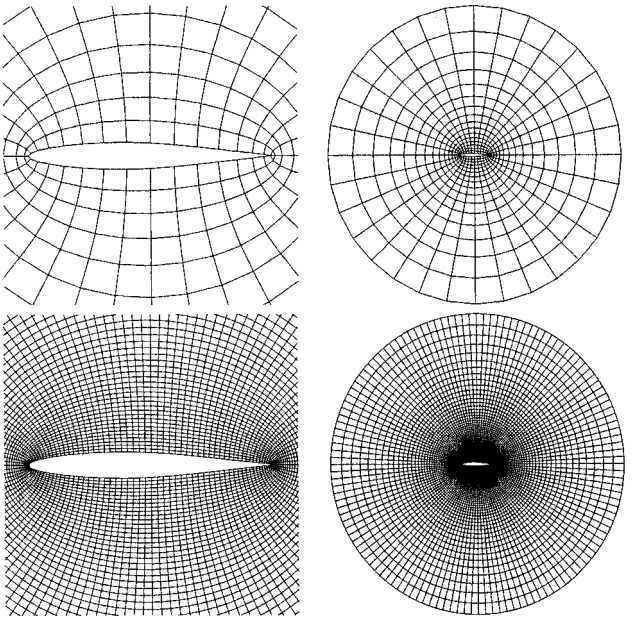

a) Grid near airfoil b) Full grid

Fig. 1 Coarse and fine computational grids for NASA Ames Research Center NACA 64A010 airfoil.

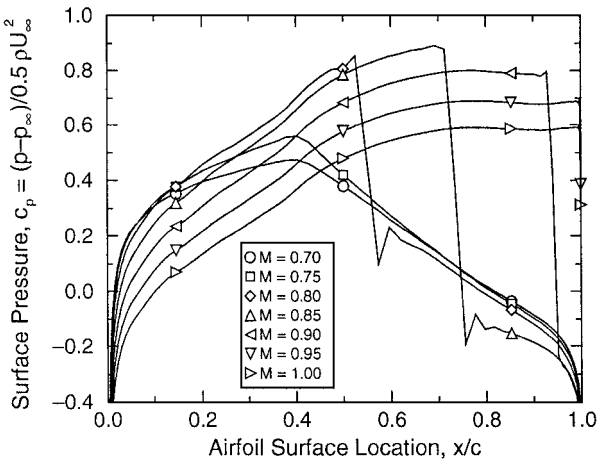

Fig. 2 Steady surface pressure distributions for NASA Ames Research Center NACA 64A010 airfoil for several freestream Mach numbers.

Having computed the snapshots, we next used the technique described in Sec. II.C to find the POD basis vectors. Figure 3 shows the eigenvalues λ of the first 41 proper orthogonal decomposition vectors. One sees the vast majority of the energy is contained in the first 10 or so POD vectors, and the energy in the modes beyond mode 15 is insignificant.

Next, the POD vectors were used to compute the eigenvalues and eigenmodes of the aerodynamic system using the Ritz-like approach given by Eq. (29) in Sec. II.D. For the first case, we retained all POD vectors in the analysis. The resulting eigenvalues are shown in Fig. 4 along with the exact eigenvalues computed by solving the generalized eigenvalue problem formed from the original CFD model, Eq. (16). For the eigenvalues near the origin, the ROM eigenvalues and the exact eigenvalues agree almost exactly. For the remaining eigenvalues, the agreement is not as good, although the qualitative shape of the eigenvalue constellations are similar.

Next, we again computed the eigenvalues using the ROM, but in this case retained the first 31 POD modes. These results are plotted in Fig. 5. In this example, a few of the smallest eigenvalues

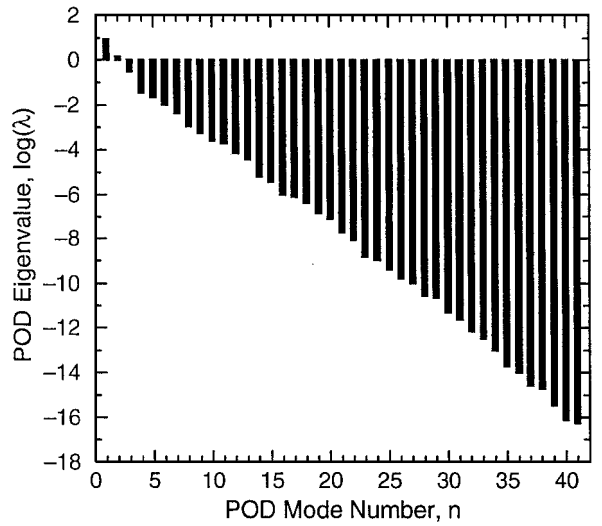

Fig. 3 Eigenvalues λ of the first 41 proper orthogonal decomposition vectors for small-disturbance flow about NASA Ames Research Center NACA 64A010 airfoil ($\alpha_0 = 0$ and $M = 0.85$) computed on coarse grid.

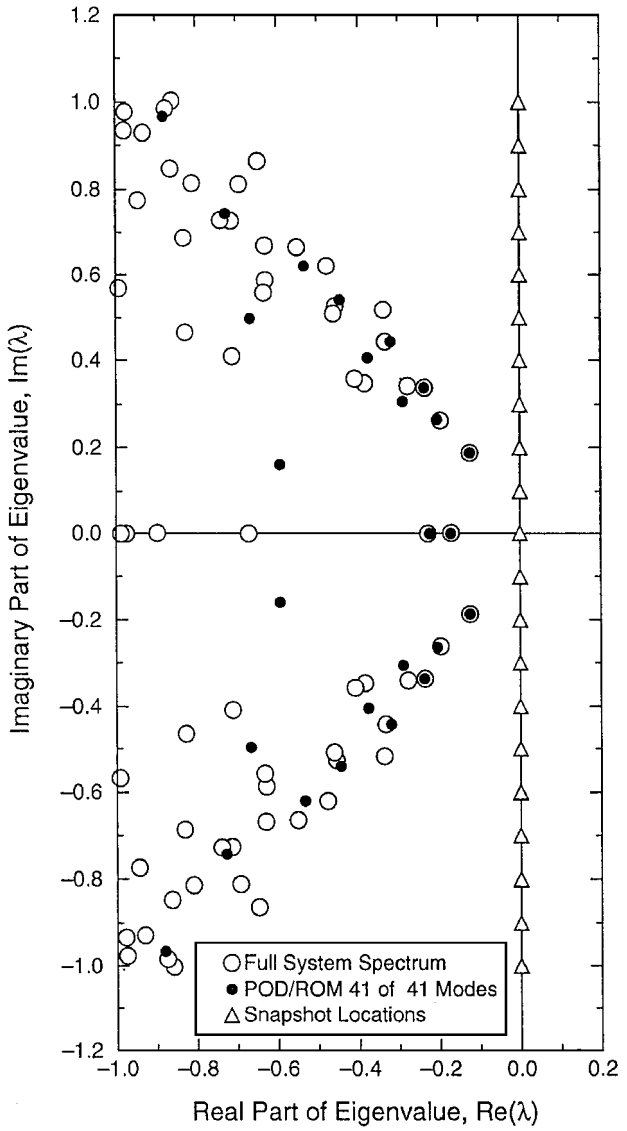

Fig. 4 Eigenspectrum of small-disturbance flow about NASA Ames Research Center NACA 64A010 airfoil ($\alpha_0 = 0$ and $M = 0.85$) computed on coarse grid; POD/ROM results computed using 41 of 41 POD modes.

are accurately computed, but many more are not. Nevertheless, the qualitative shape of the eigenvalue constellations are again similar. Similarly, Fig. 6 shows the eigenvalues computed using 21 of POD modes.

One important question regarding the construction of the reduced-order aerodynamic model is how the choice of test frequencies (not just the number of modes retained) influences the efficiency of the method. As a rule of thumb, the frequency spacing of the snapshots should be comparable or smaller than the spacing of the actual eigenvalues near the imaginary axis for the full CFD model and cannot be known a priori. One can, however, pick a somewhat arbitrary frequency spacing and compute the eigenvalues of the aerodynamic model using the POD basis vectors. If the spacing is coarse compared to the approximate eigenvalues, then one can add additional snapshots at intermediate frequencies and repeat the process until the computed eigenvalue spectrum is coarser than the snapshot spectrum.

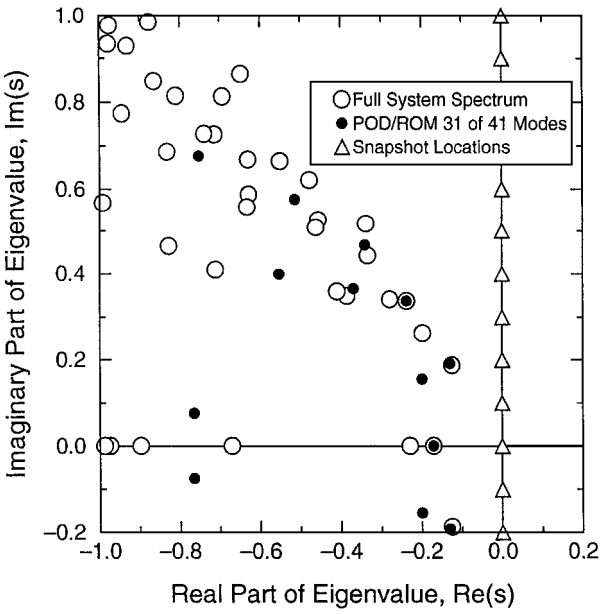

Fig. 5 Eigenspectrum of small-disturbance flow about NASA Ames Research Center NACA 64A010 airfoil ($\alpha_0 = 0$ and $M = 0.85$) computed on coarse grid; POD/ROM results computed using 31 of 41 POD modes.

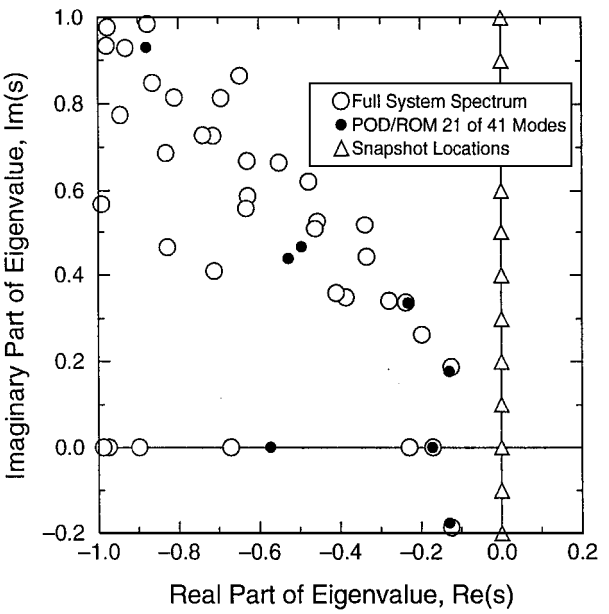

Fig. 6 Eigenspectrum of small-disturbance flow about NASA Ames Research Center NACA 64A010 airfoil ($\alpha_0 = 0$ and $M = 0.85$) computed on coarse grid; POD/ROM results computed using 21 of 41 POD modes.

Next, we use the POD basis vectors to construct the transfer function between the plunging and pitching motions of the airfoil and the resulting lift and moment. Thus, for example, to compute the transfer function between the pitching motion and lift, we prescribe a unit pitching motion at a complex frequency $\bar{\omega}$. This motion defines the vector $\boldsymbol{b}$ in Eq. (28). Equation (28) is then solved to determine ξ, the amount of each POD vector present in the unsteady small-disturbance solution. Then, by the use of Eq. (24), the entire flow field is reconstructed from the basis vectors. The unsteady surface pressure is then integrated to obtain the unsteady lift.

Figure 7 shows the transfer function for three different values of θ for a range of r, where $s = j\omega = r\exp(j\theta)$. Shown are the exact transfer function computed using the small-disturbance CFD model and the present ROM using 21 of the possible POD vectors. The present ROM is seen to be in excellent agreement with the full CFD model. A small difference between the two solutions is observed for $\theta = 120$ deg for values of r above 0.2. Similarly, Fig. 8 shows the transfer function for a ROM using just 11 of the possible POD modes. Here the ROM does not agree as well with the exact solution. However, the results are still quite acceptable for $\theta = 90$ deg, especially considering the small number of POD vectors retained in the model.

Finally, by way of comparison, we plot in Fig. 9 the pitch to lift transfer function computed using a classical Padé approximation. Here we have used the matrix Padé approximant method described by Karpel.[4] The quality of the Padé approximation is about as good as the present ROM using 11 POD vectors.

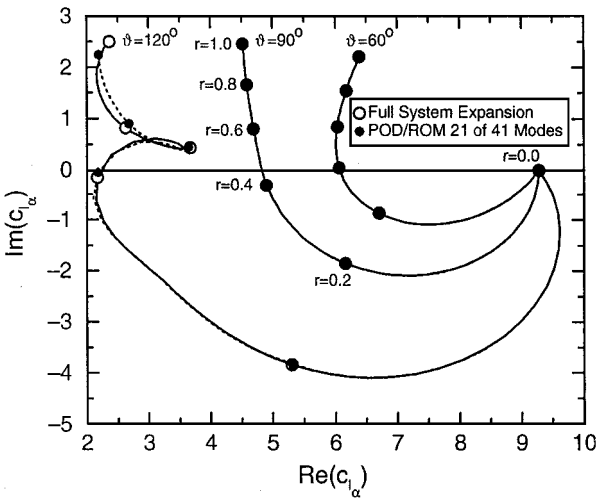

Fig. 7 Unsteady lift due to pitching motion of NASA Ames Research Center NACA 64A010 airfoil computed with 21 of 41 POD modes ($\alpha_0 = 0$ and $M = 0.85$).

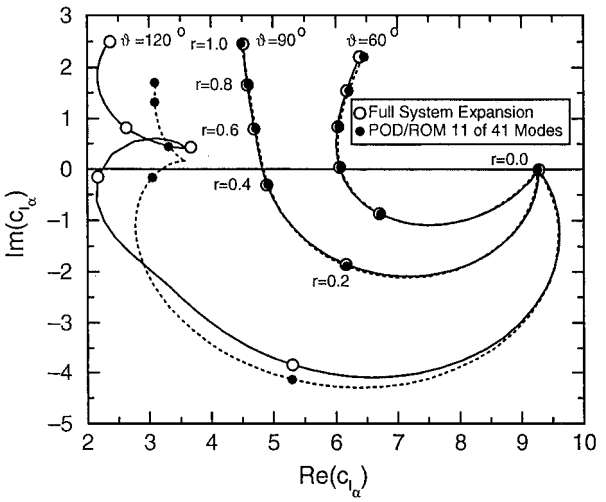

Fig. 8 Unsteady lift due to pitching motion of NASA Ames Research Center NACA 64A010 airfoil computed with 11 of 41 POD modes ($\alpha_0 = 0$ and $M = 0.85$).

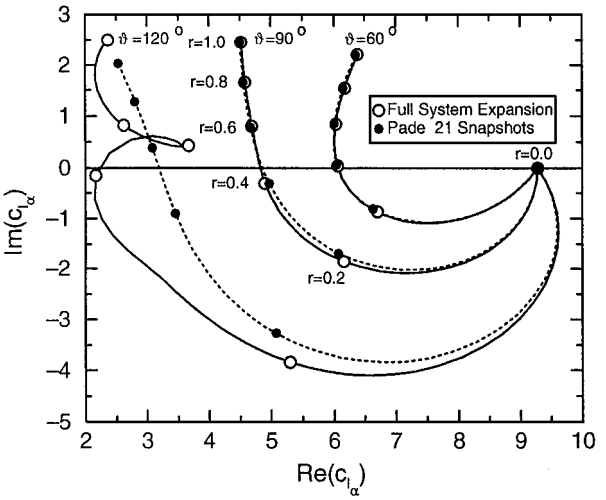

Fig. 9 Unsteady lift due to pitching motion of NASA Ames Research Center NACA 64A010 airfoil computed with matrix Padé approximant ($\alpha_0 = 0$ and $M = 0.85$).

It is of interest to note that some Padé approximants (including the one used here) increase the total number of aeroelastic degrees of freedom by a multiplicative factor times the number of structural modes. With this in mind, the minimum state method of Karpel[4] has been devised to make the aerodynamic states additive through a modification of the Padé approximant procedure. However, this is achieved at the cost of the aerodynamic transfer function being satisfied exactly at only a few frequencies. The present ROM method creates aerodynamic states that are additive to the structural states and that moreover agree exactly with the transfer function at all frequencies used to create the ROM model. Of course the present ROM model provides a consistent approximation to the eigenvalues and eigenvectors to the CFD aerodynamic model as well, whereas the Padé approximant usually prescribes the poles or eigenvalues of the Padé approximant without any knowledge of the true aerodynamic eigenvalues.

B. Unsteady Aeroelatic Behavior of a Transonic Isolated Airfoil

Next, we used the POD reduced-order modeling technique to compute the flutter boundary of the NASA Ames Research Center NACA 64A010 airfoil, using the structural dynamic parameters of Isogai's test case A (Ref. 31). Isogai chose the structural dynamic parameters to simulate the vibrational characteristics of a typical section of a swept wing. Specifically, $a = -2$, $x_\alpha = 1.8$, $r_\alpha^2 = 3.48$, $\omega_h/\omega_\alpha = 1$, and $\mu = 60$. For this series of examples, we used three different computational grids (65 × 33 nodes, 97 × 49 nodes, and 129 × 65 nodes). At each Mach number, we computed the response at 11 nondimensional frequencies $\bar{\omega}$ equally spaced between 0.0 and 1.0 for both pitching and plunging motion. Again, noting that the plunging motion solution is zero for zero frequency and that solutions for negative frequencies are complex conjugates of the solutions at positive frequencies, we obtain a total of 41 snapshots.

Figure 10 shows the root locus of the least stable eigenvalue of the reduced-order aeroelastic model given by Eq. (37) at a Mach number M of 0.85 as the reduced velocity V is varied. As the reduced velocity is increased from zero, the least stable aeroelastic eigenvalues becomes unstable (positive real part) at a reduced velocity of about 0.5. As we will see, this is the Mach number corresponding to the lowest flutter speed in the transonic dip region. As the reduced velocity is further increased, the unstable mode interestingly becomes stable again at a reduced velocity of about 2.4. This plot was computed using the finest computational mesh (129 × 65 nodes), but with ROMs constructed using 14, 21, 31, and 41 of the possible 41 POD vectors. All of these models are in good agreement. The 21, 31, and 41 vector models agree almost exactly with one another, demonstrating that the ROM is mode converged.

Next, calculations similar to those in Fig. 10 were repeated for a range of Mach numbers. Plotted in Fig. 11 is the reduced velocity at which one of the aeroelastic modes becomes neutrally stable as

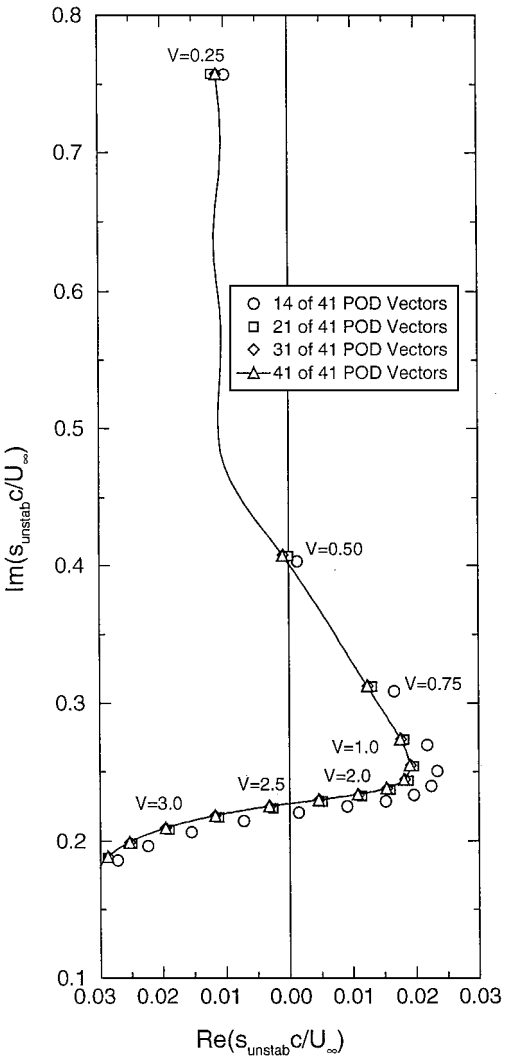

Fig. 10 Root locus of least stable aeroelastic eigenvalue of NASA Ames Research Center NACA 64A010 airfoil for a Mach number of 0.85 computed using present reduced-order model.

a function of Mach number. In Fig. 11a, we compare the results of the present ROM (129 × 65 node grid with 41 POD vectors) to the computational results of other investigators. Shown are flutter speeds predicted using transonic small-disturbance theories of Edwards et al.[32] and Isogai[31] and the time-linearized full potential theory of Ehlers and Weatherill.[33] The present method and the potential theories all show the classic transonic dip in flutter speed, although the rise in flutter speed after the dip occurs at a slightly lower Mach number in the potential theories.

To test the accuracy of the present method, we repeated this calculation, but used three different computational grid resolutions (see Fig. 11b). The flutter speeds predicted using the various computational grids are in almost exact agreement with one another. Finally, to test the modal convergence of the present ROM, we repeated the flutter speed calculation using the finest computational grid but varied the number of POD modes (14, 21, 31, or 41) used in the ROM (see Fig. 11c). All four ROMs are in good agreement, with the latter three in almost exact agreement. The results in Fig. 11b and 11c, taken together, demonstrate that the ROM has excellent grid and mode convergence properties.

C. Unsteady Aerodynamic Behvaior of a Turbomachinery Cascade

The next case we consider is that of a cascade of flat-plate two-dimensional airfoils with steady flow Mach number of 0.7. For this example, the gap-to-chord ratio G is 1.0, and the stagger angle Θ is 45 deg. Because the mass ratio μ of turbomachinery blading is very large, the flutter mechanism is not usually the frequency-coalescence type observed in aircraft wings. The unsteady aerodynamic forces

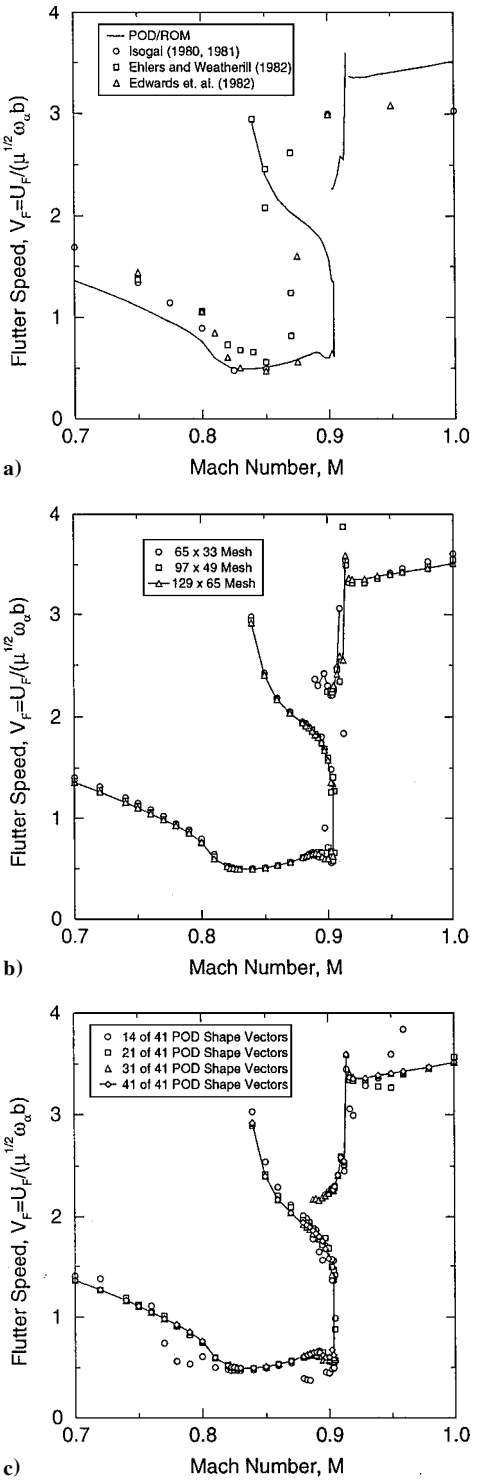

Fig. 11 Flutter speed of NASA Ames Research Center NACA 64A010 airfoil for various Mach numbers computed using reduced-order models: a) comparison of present ROM to other computational models (129 × 65 node grid with 41 POD vectors); b) present ROM with 41 POD vectors computed with coarse, medium, and fine resolution computational grids; and c) present ROM computed with fine computational grid with 12, 21, 31, and 41 POD vectors.

do not significantly alter the natural frequency or mode shape of the airfoil's vibration. However, the unsteady aerodynamic forces can provide a small amount of positive or negative aerodynamic damping. Whenever the aerodynamic damping is negative, the airfoil will flutter (in the absence of structural damping). Shown in Fig. 12 is the imaginary component of the unsteady aerodynamic moment due to pitching as a function of interblade phase angle and reduced frequency $\omega c/U_\infty$ computed using Whitehead's[34] semianalytical analysis (LINSUB). Using Whitehead's sign convention, whenever the

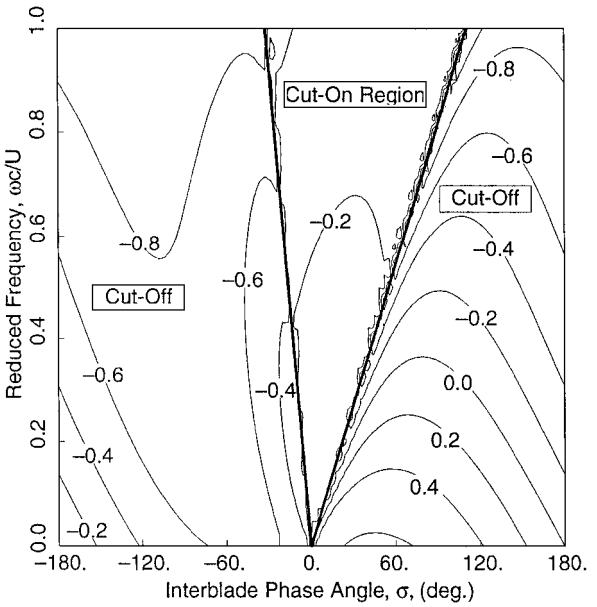

Fig. 12 Imaginary part of aerodynamic moment due to pitching of cascade of airfoils computed using Whitehead's[34] LINSUB analysis: $M = 0.7$, $G = 1$, and $\Theta = 45$ deg.

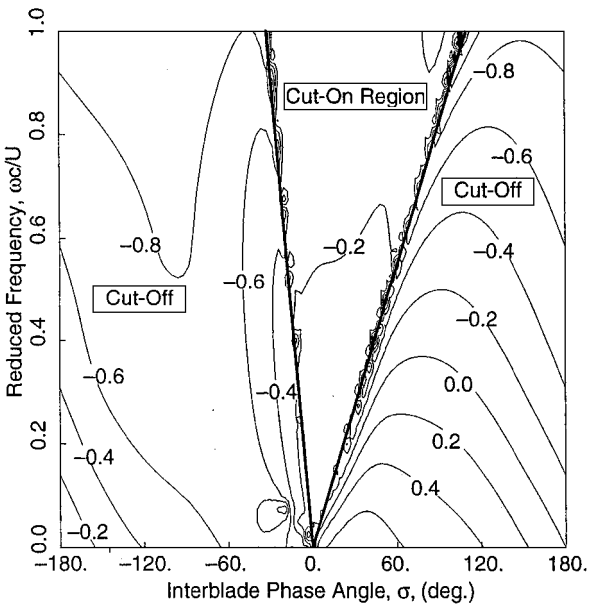

Fig. 13 Imaginary part of aerodynamic moment due to pitching of cascade of airfoils computed using POD/ROM technique with 18 of 31 POD modes: $M = 0.7$, $G = 1$, and $\Theta = 45$ deg.

imaginary part of the moment is positive, the aerodynamic damping is negative, and the cascade will flutter. One observes that there is a range of interblade phase angles between 0 and 180 deg for which the cascade will flutter at low reduced velocities).

The dark lines in Fig. 12 demark the boundary between subresonant and superresonant flow conditions. The flow is said to be superresonant whenever at least one acoustic mode is cut-on (propagates unattenuated in the axial direction) in the farfield and is subresonant otherwise. The boundary between these two regions is known as acoustic resonance; the response of the cascade changes abruptly as one passes through acoustic resonance.

Next, we constructed a reduced-order aerodynamic model for this case using the POD technique applied to a cascade version of the small-disturbance flow solver described in Sec. II.B. We computed snapshots at a combination of six reduced frequencies ($\omega c/U_\infty = 0.0$, 0.2, 0.4, 0.6, 0.8, and 1.0) and six interblade phase angles ($\sigma = -180$, -120, -60, 0, 60, and 120 deg) for a total of 36 snapshots. The POD modes of this set of solutions were computed, and the dominant 18 modes were used to construct a single ROM valid over a range of interblade phase angles and frequencies. The imaginary part of the unsteady pitching moment computed using this approach is shown in Fig. 13, and is seen to be in good agreement with the semianalytical solution of Whitehead[34] shown in Fig. 12. The overall good agreement is especially remarkable considering that only 18 aerodynamic state variables are required to model the unsteady flow over a significant range of interblade phase angles and reduced frequencies.

IV. Summary

We have described a method for constructing low-order ROMs using the proper orthogonal decomposition technique in conjunction with a time-linearized (frequency-domain) flow solver. The method has been applied to two model flow problems, that is, unsteady transonic flow about an isolated airfoil and subsonic flow through a cascade of flat-plate airfoils. In both cases, we were able to construct accurate low-order models of the unsteady flow; typical ROMs require on the order of 20 or fewer aerodynamic states. Additionally, we have shown how to couple the reduced-order aerodynamic model to a structural dynamic model to obtain a reduced-order aeroelastic model.

The major computational cost is the computation of the unsteady small-disturbance solutions (snapshots) from which the POD vectors are extracted. However, once the POD vectors have been found, the cost of constructing and solving the ROM is negligible, allowing one to quickly perform parametric studies. Unlike a conventional V–g analysis, the resulting eigenvalues are meaningful at all flow velocities above and below the flutter velocity, that is, for nonneutrally stable solutions. Furthermore, the form of the resulting ROM, with its small number of degrees of freedom, is ideally suited for use in active control applications. Although in the present paper we have applied the technique to only two-dimensional flows, the method is general and is equally applicable to three-dimensional unsteady aerodynamic and aeroelastic problems.

Acknowledgments

This work was funded through a GUIde Consortium subcontract from Carnegie Mellon University, Subcontract 537032-57209, with original funding provided through NASA John H. Glenn Research Center at Lewis Field, Contract NAS3-27735; Jerry Griffin and Anatole Kurkov are the respective Technical Monitors. This work is part of NASA's Advanced Subsonic Technology program managed by Peter Batterton and John Rohde. Additional funding was provided by Air Force Office of Scientific Research Grant F49620-97-1-0063, with Brian Sanders serving as Program Officer.

References

[1]Jones, R. T., "The Unsteady Lift of a Wing of Finite Aspect Ratio," NACA Rept. 681, 1941.

[2]Vepa, R., "On the Use of Padé Approximates to Represent Unsteady Aerodynamic Loads for Arbitrarily Small Motions of Wings," AIAA Paper 76-17, Jan. 1976.

[3]Edwards, J. W., "Applications of Laplace Transform Methods to Airfoil Motion and Stability Calculations," AIAA Paper 79-0772, April 1979.

[4]Karpel, M., "Design for Active Flutter Suppression and Gust Alleviation Using State-Space Aeroelastic Modeling," *Journal of Aircraft*, Vol. 19, No. 3, 1982, pp. 221–227.

[5]Hall, K. C., "Eigenanalysis of Unsteady Flows About Airfoils, Cascades, and Wings," *AIAA Journal*, Vol. 32, No. 12, 1994, pp. 2426–2432.

[6]Hall, K. C., Florea, R., and Lanzkron, P. J., "A Reduced Order Model of Unsteady Flows in Turbomachinery," *Journal of Turbomachinery*, Vol. 117, No. 3 1995, pp. 375–383.

[7]Florea, R., and Hall, K. C., "Eigenmode Analysis of Unsteady Flows About Airfoils," *Journal of Computational Physics*, Vol. 147, Dec. 1998, pp. 568–593.

[8]Romanowski, M. C., and Dowell, E. H., "Reduced Order Euler Equations for Unsteady Aerodynamic Flows: Numerical Techniques," AIAA Paper 96-0528, Jan. 1996.

[9]Dowell, E. H., Hall, K. C., and Romanowski, M. C., "Eigenmode Analysis in Unsteady Aerodynamics: Reduced Order Models," *Applied Mechanics Review*, Vol. 50, No. 6, 1997, pp. 371–386.

[10]Loève, M., *Probability Theory*, D. Van Nostrand, New York, 1955.

[11]Lumley, J. L., "The Structures of Inhomogeneous Turbulent Flow," *Atmospheric Turbulence and Radio Wave Propagation*, edited by A. M. Yaglom and V. I. Tatarski, Nauka, Moscow, 1967, pp. 166–178.

[12]Berkooz, G., Holmes, P., and Lumley, J. L., "The Proper Orthogonal Decomposition in the Analysis of Turbulent Flows," *Annual Review of Fluid Mechanics*, Vol. 25, 1993, pp. 539–575.

[13]Poje, A. C., and Lumley, J. L., "A Model for Large-Scale Structures in Turbulent Shear Flows," *Journal of Fluid Mechanics*, Vol. 285, Feb. 1995, pp. 349–369.

[14]Sirovich, L., "Turbulence and the Dynamics of Coherent Structures, Part I: Coherent Structures," *Quarterly of Applied Mathematics*, Vol. 45, No. 3, 1987, pp. 561–571.

[15]Sirovich, L., "Turbulence and the Dynamics of Coherent Structures, Part II: Symmetries and Transformations," *Quarterly of Applied Mathematics*, Vol. 45, No. 3, 1987, pp. 573–582.

[16]Sirovich, L., "Turbulence and the Dynamics of Coherent Structures, Part III: Dynamics and Scaling," *Quarterly of Applied Mathematics*, Vol. 45, No. 3, 1987, pp. 583–590.

[17]Moin, P., and Moser, R. D., "Characteristic-Eddy Decomposition of Turbulence in a Channel," *Journal of Fluid Mechanics*, Vol. 200, March 1989, pp. 471–509.

[18]Rempfer, D., and Fasel, H., "Evolution of Three-Dimensional Coherent Structures in a Flat-Plate Boundary Layer," *Journal of Fluid Mechanics*, Vol. 260, Feb. 1994, pp. 351–375.

[19]Rempfer, D., and Fasel, H., "Dynamics of Three-Dimensional Coherent Structures in a Flat-Plate Boundary Layer," *Journal of Fluid Mechanics*, Vol. 275, Sept. 1994, pp. 257–283.

[20]Deane, A. E., Kevrekidis, I. G., Karniadakis, G. E., and Orszag, S. A., "Low-Dimensional Models for Complex Geometry Flows: Application to Grooved Channels and Circular Cylinders," *Physics of Fluids A*, Vol. 3, No. 10, 1991, pp. 2337–2354.

[21]Holmes, P., Lumley, J. L., and Berkooz, G., *Turbulence, Coherent Structures, Dynamical Systems and Symmetry*, Cambridge Univ. Press, Cambridge, England, U.K., 1996.

[22]Romanowski, M. C., "Reduced Order Unsteady Aerodynamic and Aeroelastic Models Using Karhunen–Loève Eigenmodes," AIAA Paper 96-3981, 1996.

[23]Tang, K. Y., Graham, W. R., and Peraire, J., "Active Flow Control Using a Reduced Order Model and Optimum Control," AIAA Paper 96-1946, 1996.

[24]Kim, T., "Frequency-Domain Karhunen-Loève Method and Its Application to Linear Dynamic Systems," *AIAA Journal*, Vol. 36, No. 11, 1998, pp. 2117–2123.

[25]Hall, K. C., and Clark, W. S., "Linearized Euler Predictions of Unsteady Aerodynamic Loads in Cascades," *AIAA Journal*, Vol. 31, No. 3, 1993, pp. 540–550.

[26]Godunov, S. K., "A Finite Difference Method of the Numerical Computation of Discontinuous Solutions of the Equations of Fluid Dynamics," *Matematicheskii Sbornik*, Vol. 47, 1959, pp. 357–393.

[27]Roe, P. L., "Approximate Riemann Solvers, Parameter Vectors, and Difference Schemes," *Journal of Computational Physics*, Vol. 43, 1981, pp. 357–372.

[28]van Leer, B., "Towards the Ultimate Conservative Difference Scheme, II, Monotonicity and Conservation Combined in a Second-Order Scheme," *Journal of Computational Physics*, Vol. 14, 1974, pp. 361–376.

[29]Ni, R. H., "A Multiple-Grid Scheme for Solving the Euler Equations," *AIAA Journal*, Vol. 28, No. 12, 1982, pp. 2050–2058.

[30]Bland, S. R., "AGARD Two-Dimensional Aeroelastic Configurations," AR-156, AGARD, Aug. 1979.

[31]Isogai, K., "On the Transonic-Dip Mechanism of Flutter of Sweptback Wing," *AIAA Journal*, Vol. 17, No. 7, 1979, pp. 793–795.

[32]Edwards, J. W., Bennett, R. M., Whitlow, W., Jr., and Seidel, D. A., "Time-Marching Transonic Flutter Solutions Including Angle-of-Attack Effects," *Journal of Aircraft*, Vol. 20, No. 11, 1983, pp. 899–906.

[33]Ehlers, F. E., and Weatherill, W. H., "A Harmonic Analysis Method for Unsteady Transonic Flow and Its Application to the Flutter of Airfoils," NASA CR-3537, May 1982.

[34]Whitehead, D. S., "Classical Two-Dimensional Methods," *AGARD Manual on Aeroelasticity in Axial Flow Turbomachines, Vol. 1: Unsteady Turbomachinery Aerodynamics*, edited by M. F. Platzer and F. O. Carta, Vol. 1, AG-298, AGARD, 1987, Chap. 3.

P. Givi
Associate Editor